Far-field acoustic holography onto cylindrical surfaces using pressure measured on semicircles

Andrew N. Norris

Department of Mechanical and Aerospace Engineering, Rutgers University, Piscataway, New Jersey 08855-0909

(Received 25 April 1997; revised 7 July 1997; accepted 8 July 1997)

A simple formula was recently proposed by Williams [J. Acoust. Soc. Am. 99, 2022–2032 (1996)] for imaging pressure and velocity on a vibrating circular cylindrical shell using the far-field pressure measured along a meridional semicircle. The method is examined and some new results are obtained. The procedure is generalized to handle cylindrical surfaces of noncircular but convex cross section. It is demonstrated that Williams' formula predicts a supersonic surface intensity which gives the same meridional energy flux as the exact radiated far-field pressure. A modification of Williams' formula is suggested which uses pressure data from several neighboring semicircles, although complete spherical coverage is not required. The modified imaging formula is based upon the first two terms in an asymptotic expansion in the dimensionless wave number. The leading-order term yields the original formula, and the second term results in a boundary layer type of correction in the circumferential direction. Numerical examples are presented which compare the exact supersonic acoustic intensity on a cylinder with that from the original and the modified formula. These indicate that the circumferential on-surface resolution is significantly enhanced by combining data from neighboring semicircles, even when the total far-field spherical coverage is small. © 1997 Acoustical Society of America. [\$0001-4966(97)05110-2]

PACS numbers: 43.30.Jx, 43.20.Rz, 43.40.Rj, 43.35.Sx [SAC-B]

INTRODUCTION

Acoustic holography provides a powerful tool for visualizing and understanding the vibration on a structure using pressure measured in the near or far field. Near-field data is preferred, in the sense that it includes information about the evanescent, subsonic pressure field which does not radiate to the far field. The theory and practice of near-field acoustic imaging has developed considerably in the past decade, beginning with Williams et al. who presented the details for the specific case of the circular cylindrical geometry, including the necessary wave-number filtering. Veronesi and Maynard² subsequently described a method for reconstructing data on nonseparable surfaces using singular value decomposition. Borgiotti et al.³ discussed numerical applications of the SVD technique for surfaces conforming to a nonseparable closed surface, and they provided accuracy estimates based on the dynamic range of the data.

Far-field acoustic holography for cylindrical and nonseparable surfaces has received less attention. This may be ascribed to the loss in information caused by the radiation process: short wavelength or subsonic surface data does not radiate, and one is left with the filtered supersonic data. Sarkissian⁴ proposed a general scheme for reconstructing surface velocity on arbitrary surfaces from far-field data. The method relies upon impedance eigenfunctions for the surface, which form a complete and orthogonal basis for the far-field radiation pattern. This functional basis is also related to the singular value decomposition of the impedance operator. However, except for separable surfaces, the set of basis functions must be determined numerically, with increasing difficulty at higher frequencies. Furthermore, the radiation operator which maps surface data to a far-field radiation pattern is a compact operator, and its inversion is an ill-posed process, implying that far-field reconstruction of surface data is itself an ill-posed problem.

Recently, Williams⁶ showed that a very simple but approximate technique yields surprisingly accurate imaging. The method is specifically for circular cylindrical surfaces, and uses far-field pressure data measured on meridional semicircles to image the surface pressure and velocity in the same plane. Williams provided an extensive comparison of the exact and approximate images, using simulated data and near-field versus far-field experimental data. He also showed that the imaging formula can be derived from the exact equations for the circular cylindrical geometry. Overall, the accuracy is remarkable over a wide frequency range (ka =0.3-16.0). The only limitation is that the surface data should be bandlimited in the circumferential, or azimuthal, direction, roughly $n \le ka/3$. However, the numerical and experimental comparisons are surprisingly good even for a point drive on the cylinder.

In this paper we will examine the imaging formula from a slightly different perspective. It will be demonstrated that the formula is a simple consequence of a high-frequency approximation. This is implicit in Williams' analysis also, but here we show how the high-frequency nature of the approximation makes it equally applicable to cylinders of arbitrary nonseparable cross section. As with many highfrequency approximations, this one also proves to be accurate for frequencies such that ka is not large, even of order unity. The approach taken here is based upon the Helmholtz surface integral, which allows us to find the leading-order asymptotic approximation for the far-field pattern function. This is derived in the next section, followed by

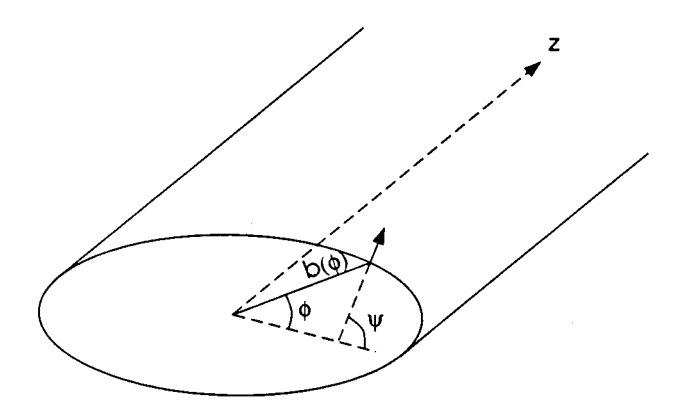


FIG. 1. The cylinder cross section and geometrical parameters.

a discussion of energy conservation. An improvement, based upon the next term in the asymptotic series, is presented in Sec. II for the specific case of a circular cylinder. The new scheme uses data from neighboring circles to give improved circumferential accuracy. Finally, the method is illustrated by examples and alternative numerical implementations are discussed.

I. THE SIMPLE IMAGING FORMULA

A. Derivation

We will work primarily with cylindrical polar coordinates $\mathbf{x} = (\rho, z, \phi)$ but also use spherical polar coordinates $\mathbf{x} = (r, \theta, \phi)$ where $r^2 = \rho^2 + z^2$ and $z = r \cos \theta$. The acoustic pressure is assumed to radiate from sources on or within a cylinder of constant cross section C defined by the radius $\rho = b(\phi)$ and sufficiently long in the z direction that end effects may be ignored, see Fig. 1. We assume that the cylinder cross section is convex and smooth. The far-field pattern function F is defined by

$$p(r,\theta,\phi) = \frac{e^{ikr}}{r} F(\theta,\phi) + O\left(\frac{1}{r^2}\right), \quad r \to \infty,$$
 (1)

where $e^{-i\omega t}$ dependence is assumed. Our objective is to image the acoustic field on the cylindrical surface using F. It is well known that only those components of the surface pressure and velocity which are supersonic can radiate to the far field. Let $f(b(\phi), z, \phi)$ represent a quantity on the surface $\rho = b(\phi)$, such as pressure or velocity. It may be partitioned into supersonic and subsonic parts, $f^{(s)}(z, \phi)$ and $f^{(c)} \times (z, \phi)$, respectively, such that $f = f^{(s)} + f^{(c)}$ and

$$f^{(s)}(z,\phi) = \int_{-\infty}^{\infty} dz' \ f(b(\phi),z',\phi) \ \frac{\sin[k(z-z')]}{\pi(z-z')}. \tag{2}$$

The supersonic surface pressure and normal velocity on $\rho = b(\phi)$ are defined in the same way as $p^{(s)}(z,\phi)$ and $v^{(s)} \times (z,\phi)$, respectively. The basic formula that we will derive is for $\hat{p}^{(s)}$, which approximates $p^{(s)}$ (the hat denotes an approximant of a quantity)

$$\hat{p}^{(s)}(z,\phi) = e^{i\pi/4} \sqrt{\frac{k}{2\pi a(\phi)}} \int_0^{\pi} d\theta \sqrt{\sin\theta} \times e^{ik(b(\phi)\sin\theta + z\cos\theta)} F(\theta, \psi(\phi)). \tag{3}$$

Here $a(\phi)$ is the radius of curvature at the position ϕ , and the $\psi(\phi)$ is the angle for the normal, see Fig. 1. Let $l(\phi)$ denote the arclength on the curve defining the cross section, i.e., $dl/d\phi = \sqrt{b^2 + (db/d\phi)^2}$, then

$$a(\phi) = \frac{dl}{d\psi}, \quad \psi(\phi) = \phi - \tan^{-1}\left(\frac{1}{b}\frac{db}{d\phi}\right).$$
 (4)

Equation (3) reproduces Williams' formula [Eq. (17) of Ref. 6] for the special case of a circular cylinder ($b \equiv a = \text{constant}$). Williams also obtained a simple formula for the supersonic radial velocity on the circular cylinder [Eq. (18) of Ref. 6]. The analogous result for the general cross section is

$$\hat{v}^{(s)}(z,\phi) = \frac{e^{i\pi/4}}{\rho_f c} \sqrt{\frac{k}{2\pi a(\phi)}} \int_0^{\pi} d\theta (\sin\theta)^{3/2} \times e^{ik(b(\phi)\sin\theta + z\cos\theta)} F(\theta, \psi(\phi)), \tag{5}$$

where ρ_f is the fluid density and $c = \omega/k$ the acoustic wave speed.

Williams⁶ derived his formulas for the circular cylinder using an exact representation for the supersonic fields in terms of the far-field pressure. Here we present an alternative derivation which does not rely upon an azimuthal modal expansion explicitly. We start with the Helmholtz integral formula of the radiated acoustic pressure in terms of the pressure and normal velocity on the cylindrical surface,

$$p(\rho, z, \phi) = \int_{C} dl \int_{-\infty}^{\infty} dz' \bigg[p(b(\phi'), z', \phi')$$

$$\times \frac{\partial g}{\partial n} (\rho, z, \phi; b(\phi'), z', \phi')$$

$$-i\omega \rho_{f} v(b(\phi'), z', \phi') g(\rho, z, \phi; b(\phi'), z', \phi') \bigg],$$
(6)

where $g(\rho, z, \phi; \rho', z', \phi') = (4\pi R)^{-1} e^{ikR}$, $R = |\mathbf{x} - \mathbf{x}'|$. This implies that the far-field form function has the exact representation

$$F(\theta,\phi) = \frac{-ik}{4\pi} \int_{C} dl \int_{-\infty}^{\infty} dz' \ e^{-ik(z'\cos\theta + b(\phi')\sin\theta\cos(\phi - \phi'))}$$

$$\times [\rho_{f} cv(b(\phi'), z', \phi') + \sin\theta\cos(\phi - \psi(\phi'))p(b(\phi', z', \phi')]. \tag{7}$$

By transforming in z, we obtain

$$F(\theta,\phi) = \frac{-ik}{4\pi} \int_{C} dl \ e^{-ikb(\phi')\sin\theta\cos(\phi-\phi')}$$

$$\times [\rho_{f}cV(k\cos\theta,\phi') + \sin\theta\cos(\phi')]$$

$$-\psi(\phi')P(k\cos\theta,\phi')], \tag{8}$$

where the transforms are

$$\begin{pmatrix} P(k_z, \phi) \\ V(k_z, \phi) \end{pmatrix} = \int_{-\infty}^{\infty} dz \ e^{-ik_z z} \begin{pmatrix} p(b(\phi), z, \phi) \\ v(b(\phi), z, \phi) \end{pmatrix}. \tag{9}$$

The supersonic surface fields can also be expressed in terms of the z transforms as

$$\begin{pmatrix} p^{(s)}(z,\phi) \\ v^{(s)}(z,\phi) \end{pmatrix} = \frac{k}{2\pi} \int_0^{\pi} d\theta \\
\times \sin \theta e^{ikz \cos \theta} \begin{pmatrix} P(k \cos \theta,\phi) \\ V(k \cos \theta,\phi) \end{pmatrix}, \quad (10)$$

since Eqs. (9) and (10) are together equivalent to Eq. (2). Our objective is to derive approximations to $P(k \cos \theta, \phi)$ and $V(k \cos \theta, \phi)$. With this in mind we make two assumptions. (i) First, we assume the normal velocity and pressure are related by a "cylindrical wave" approximation, which is most easily expressed in terms of the transformed variables as

$$\hat{V}(k \cos \theta, \phi) = \frac{\sin \theta}{\rho_f c} \hat{P}(k \cos \theta, \phi) \left\{ 1 - \frac{1}{2ika(\phi)\sin \theta} + O\left(\frac{1}{(ka \sin \theta)^2}\right) \right\}.$$
(11)

This may be justified by the high-frequency approximation for the z-transformed pressure $P(\rho_n, k_z, \phi)$ near the surface, where ρ_n is the distance from C in the normal direction,

$$P(\rho_n, k_z, \phi) = P(k_z, \phi) e^{i\sqrt{k^2 - k_z^2}\rho_n} \times \sqrt{\frac{a(\phi)}{a(\phi) + \rho_n}} \left[1 + O\left(\frac{1}{ka}\right) \right].$$
 (12)

Thus using $V(\rho_n, k_z, \phi) = (i\omega\rho_f)^{-1}\partial P/\partial \rho_n$, and evaluating on the surface $(\rho_n = 0)$, we get Eq. (11). This approximation is justified further for the circular cylinder in the Appendix. (ii) Second, we assume that we may perform asymptotic expansions in the large parameter $ka \sin \theta \gg 1$. This was already implicit in the cylindrical wave approximation of Eq. (11).

Equations (3) and (5) can now be derived. First, substituting from Eq. (11) into the exact formula (8) and retaining only the leading order term, we have

$$\hat{F}(\theta,\phi) = \frac{-ik}{4\pi} \int_{C} dl \ e^{-ikb(\phi')\sin\theta\cos(\phi - \phi')} [1 + \cos(\phi - \psi(\phi'))] \sin\theta P(k\cos\theta,\phi'). \tag{13}$$

We now apply the stationary phase approximation to this integral, based upon the assumption that $ka \sin \theta \gg 1$. There are two points at which the phase is stationary, given by the implicit relations $\psi(\phi') = \phi$ and $\psi(\phi') = \phi + \pi$. However, the integrand vanishes at the latter point and we get zero contribution there. The remaining stationary phase point gives

$$\hat{F}(\theta, \psi(\phi)) = e^{-i\pi/4} e^{-ikb(\phi)\sin\theta}$$

$$\times \sqrt{\frac{ka(\phi)\sin\theta}{2\pi}} P(k\cos\theta, \phi), \qquad (14)$$

or

$$\hat{P}(k \cos \theta, \phi) = e^{i\pi/4} e^{ikb(\phi)\sin \theta}$$

$$\times \sqrt{\frac{2\pi}{ka(\phi)\sin \theta}} F(\theta, \psi(\phi)). \tag{15}$$

Substituting from Eq. (15) into Eq. (10) yields the imaging formula (3). The velocity formula (5) follows in the same way using the leading-order term of the cylindrical wave approximation (11).

B. Conservation of radiated energy

The flux of energy across the cylindrical surface at a point is defined as the time averaged power flow:

$$I(z,\phi) = \frac{1}{2} \operatorname{Re}[p(b(\phi),z,\phi)v^*(b(\phi),z,\phi)], \tag{16}$$

and the supersonic acoustic intensity is defined as the contribution from the supersonic components:

$$I^{(s)}(z,\phi) = \frac{1}{2} \text{Re}[p^{(s)}(z,\phi)v^{(s)}*(z,\phi)]. \tag{17}$$

Similarly, one can define a subsonic flux, $I^{(c)}(z,\phi)$, using the subsonic surface fields $p^{(c)}(z,\phi)$ and $v^{(c)}(z,\phi)$. Note that $I(z,\phi) \neq I^{(s)}(z,\phi) + I^{(c)}(z,\phi)$ in general. However, by the definition of the supersonic component, Eq. (2), it follows that

$$\int_{-\infty}^{\infty} dz \, f^{(s)}(z, \phi) g^{(c)}(z, \phi) = 0 \tag{18}$$

for any surface fields f and g, and hence

$$\int_{-\infty}^{\infty} dz \ I(z,\phi) = \int_{-\infty}^{\infty} dz \ I^{(s)}(z,\phi) + \int_{-\infty}^{\infty} dz \ I^{(c)}(z,\phi).$$
(19)

Assuming that all sources lie on or within the surface implies that the total subsonic flux is zero, and hence

$$\int_{C} dl \int_{-\infty}^{\infty} dz \ I(z, \phi) = \int_{C} dl \int_{-\infty}^{\infty} dz \ I^{(s)}(z, \phi) = \Pi(\omega),$$
(20)

where $\Pi(\omega)$ is the total energy radiated to the far field,

$$\Pi(\omega) = \frac{1}{2\rho_f c} \int_0^{2\pi} d\phi \int_0^{\pi} d\theta \sin \theta |F(\theta, \phi)|^2.$$
 (21)

We now demonstrate that the imaging formulas have the useful property that they conserve energy. Replacing $p^{(s)}$ and $v^{(s)}$ by the integral expressions of Eq. (10), then integrating in the axial coordinate z and using known properties of the Dirac delta function, we obtain the identity

$$\int_{-\infty}^{\infty} dz \ I^{(s)}(z,\phi) = \frac{k}{4\pi} \int_{0}^{\pi} d\theta \sin \theta \operatorname{Re}[P(k \cos \theta, \phi)] \times V^{*}(k \cos \theta, \phi)]. \tag{22}$$

As a first approximation, the cylindrical wave, or local impedance condition, of Eq. (11) combined with Eq. (22) implies

$$\int_{-\infty}^{\infty} dz \ I^{(s)}(z,\phi) = \frac{k}{4\pi\rho_f c} \int_{0}^{\pi} d\theta \sin^2\theta |P(k\cos\theta,\phi)|^2$$
$$\times \left[1 + O\left(\frac{1}{(ka)^2}\right)\right]. \tag{23}$$

If we now substitute the leading-order approximation for $P(k \cos \theta, \phi)$ from Eq. (15), we obtain

$$\int_{-\infty}^{\infty} dz \hat{I}^{(s)}(z,\phi) = \frac{1}{2a(\phi)\rho_f c} \int_{0}^{\pi} d\theta \sin \theta |F(\theta,\psi(\phi))|^2.$$
(24)

Hence using the relation $dl = ad\psi$ [see Eq. (4)], we see that the surface energy flux of the approximate imaged field,

$$a(\phi) \int_{-\infty}^{\infty} dz \ \hat{I}^{(s)}(z,\phi), \tag{25}$$

exactly equals the differential power radiated per unit azimuthal angle in the far field in the direction $\psi(\phi)$. Thus we have energy conservation for each meridional patch of width dl and of infinite length, $-\infty < z < \infty$. According to Eq. (19), the exact supersonic flux corresponding to (25) is not necessarily the same as the net flux from the patch. The identity only holds for the entire surface. However, the cylindrical wave approximation implies that each patch radiates independently of all others. In this regard, we note that Sarkissian⁸ introduced the idea of far-field eigenfunctions, which have a one-to-one relation with the on-surface eigenfunctions of the real part of the impedance operator. According to the present level of approximation, the patches and the velocity on them represent orthogonal subspaces of these eigenfunctions.

The following is a simple consequence of the preceding analysis,

$$\int_{C} dl \int_{-\infty}^{\infty} dz \ \hat{I}^{(s)}(z, \phi) = \Pi(\omega). \tag{26}$$

In summary, Williams' formulas and their generalization to arbitrary cross-sections predict a supersonic acoustic intensity which gives the same local energy flux on a longitudinal patch as the differential far-field intensity, and the same global energy flux as the exact radiated pressure. In this sense the imaging formulas are energy preserving.

II. AN ASYMPTOTIC CORRECTION FOR THE CIRCULAR CYLINDER

A. Analysis

The preceding analysis showed that Williams' formula is based upon the leading-order asymptotic approximation of the exact integral (8) for F. In order to improve upon this result we now explore the possibility of extending the formula by retaining the subsequent term in the asymptotic expansion. For simplicity, we restrict the analysis to the circular cylinder (b=a) but use the same methodology as before,

based upon the Helmholtz integral. The case of variable $b(\phi)$ can be treated similarly. The Appendix summarizes the same analysis using the explicit circular functions.

Here, the asymptotic parameter turns out to be $ka \sin \theta$, which may not be large if θ is near 0 or π . However, we will proceed by ignoring these limiting values, and start by considering the integral

$$f(\phi) = \int_0^{2\pi} d\phi' \ g(\phi') e^{-ika \sin \theta \cos(\phi - \phi')}, \tag{27}$$

where $g(\phi)$ is assumed to be reasonably smooth. Our objective is to obtain the two leading-order terms in the asymptotic expansion of $f(\phi)$. The integral (27) can be put into a form suitable for asymptotic approximation by introducing the dimensionless large parameter $\lambda = 2\sqrt{ka} \sin \theta$, so that with a change of variable

$$f(\phi) = \frac{2}{\lambda} e^{-i\lambda^2/4} \int_{-\lambda}^{\lambda} dx \frac{e^{ix^2/2}}{\sqrt{1 - x^2/\lambda^2}} g\left[\phi + 2\sin^{-1}\left(\frac{x}{\lambda}\right)\right]. \quad (28)$$

Expanding the integrand about x = 0 in terms of inverse powers of λ gives

$$f(\phi) = \frac{2}{\lambda} e^{-i\lambda^{2}/4} \int_{-\lambda}^{\lambda} dx \ e^{ix^{2}/2} \left\{ g(\phi) + 2\frac{x}{\lambda} g'(\phi) + \frac{x^{2}}{2\lambda^{2}} [g(\phi) + 4g''(\phi)] + O(\lambda^{-3}) \right\}$$

$$= \frac{2}{\lambda} e^{-i\lambda^{2}/4} \left\{ K_{\lambda}(1)g(\phi) - \frac{i}{\lambda^{2}} K_{\lambda}'(1)[g(\phi) + 4g''(\phi)] + O(\lambda^{-3}) \right\}, \tag{29}$$

where

$$K_{\lambda}(\alpha) = \int_{-\lambda}^{\lambda} dx \ e^{i\alpha x^2/2}.$$
 (30)

The function $K_{\lambda}(\alpha)$ may be expressed in terms of known functions, but for our purposes it suffices to take the large λ limit, $K_{\infty}(\alpha) = e^{i\pi/4} \sqrt{2\pi/\alpha}$, so that

$$f(\phi) = e^{i(\pi/4 - ka \sin \theta)} \sqrt{\frac{2\pi}{ka \sin \theta}} \left\{ g(\phi) - \frac{1}{2ika \sin \theta} \times \left[g''(\phi) + \frac{1}{4} g(\phi) \right] + O\left(\frac{1}{(ka \sin \theta)^{3/2}}\right) \right\}.$$
(31)

Equation (8) for F involves two distinct integrals for the integrands V and P, and Eq. (31) can be applied to each integral separately. However, we would like to obtain an expression for F which contains only one of the two integrands. This can be achieved to within the desired asymptotic accuracy by using the cylindrical wave approximation of Eq. (11). Substituting from (11) into the integral (8) and using the asymptotic approximation (31) we obtain

$$\hat{F}(\theta,\phi) = e^{-i(ka\sin\theta + \pi/4)} \sqrt{\frac{ka\sin\theta}{2\pi}} \left[P(k\cos\theta,\phi) - \frac{1}{2ika\sin\theta} \left(P_{,\phi\phi}(k\cos\theta,\phi) + \frac{1}{4}P(k\cos\theta,\phi) \right) + O\left(\frac{1}{(ka\sin\theta)^{3/2}}\right) \right].$$
(32)

This is the first-order correction of the leading-order approximation of Eq. (14). It is interesting to note that there is still no contribution to the far field from the stationary phase point at $\phi + \pi$. That is, the approximation (32) is still local, although it now involves the second derivative of the surface pressure transform.

B. Discussion and examples

Equation (32) was derived as an asymptotic correction of the leading-order term, and as such, we may formally invert it as

$$\hat{P}(k \cos \theta, \phi) = e^{i\pi/4} e^{ika \sin \theta} \sqrt{\frac{2\pi}{ka \sin \theta}}$$

$$\times \left[\left(1 + \frac{1}{8ika \sin \theta} \right) F(\theta, \phi) + \frac{1}{2ika \sin \theta} F_{,\phi\phi}(\theta, \phi) + O\left(\frac{1}{(ka \sin \theta)^{3/2}} \right) \right]. \tag{33}$$

This gives the following approximation for the supersonic surface pressure,

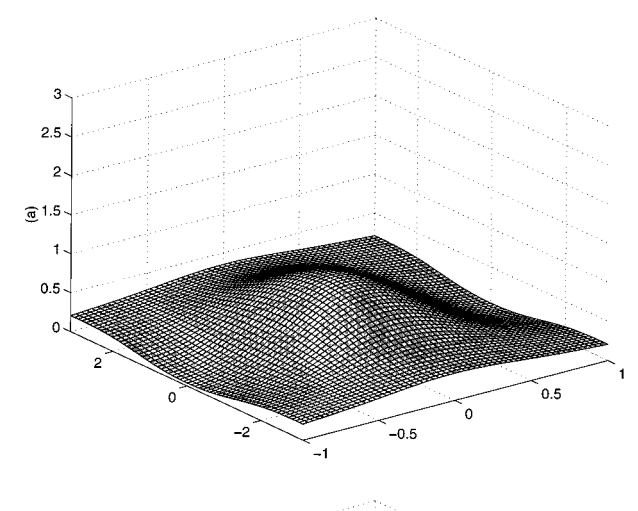
$$\hat{p}^{(s)}(z,\phi) = e^{i\pi/4} \sqrt{\frac{k}{2\pi a}} \int_0^{\pi} \frac{d\theta}{\sqrt{\sin\theta}} e^{ik(a\sin\theta + z\cos\theta)} \times \left[\left(\sin\theta + \frac{1}{8ika} \right) F(\theta,\phi) + \frac{F_{,\phi\phi}(\theta,\phi)}{2ika} \right].$$
(34)

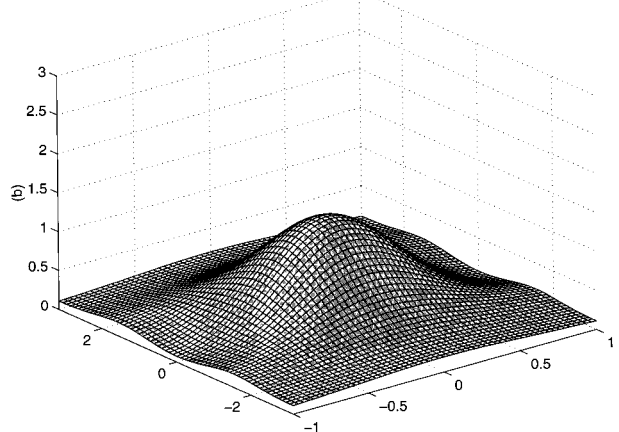
The corresponding approximation for the supersonic surface velocity is, from (11) and (33),

$$\hat{v}^{(s)}(z,\phi) = \frac{e^{i\pi/4}}{\rho_f c} \sqrt{\frac{k}{2\pi a}} \int_0^{\pi} d\theta \sqrt{\sin\theta} e^{ik(a\sin\theta + z\cos\theta)} \times \left[\left(\sin\theta - \frac{3}{8ika} \right) F(\theta,\phi) + \frac{F_{,\phi\phi}(\theta,\phi)}{2ika} \right].$$
(35)

We will test the accuracy of the imaging formulas for a monopole at $(\rho, z, \phi) = (\rho', 0, 0)$, $\rho' < a$, for which

$$F(\theta, \phi) = e^{-ik\rho' \sin \theta \cos \phi}.$$
 (36)





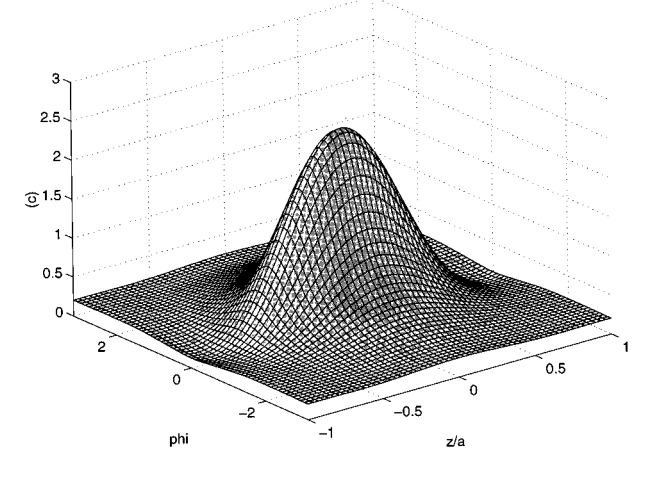


FIG. 2. The supersonic acoustic intensity for $\rho' = 0.5a$ and ka = 3, computed using (a) the simple formulas of Eqs. (3) and (5), (b) Eqs. (34) and (35), and (c) the exact result.

The exact supersonic surface pressure can be obtained using the identity (A11). Figures 2 and 3 compare the predicted supersonic acoustic intensity according to the simple formulas of Williams, Eqs. (3) and (5), and the "improved" versions (34) and (35), with the exact supersonic acoustic intensity for a source at $\rho' = a/2$ for ka = 3. The amplitudes of the approximations are lower near the center of the image ($z = \phi = 0$) than the exact intensity, but the "improved" imaging formula does appear to give better resolution.

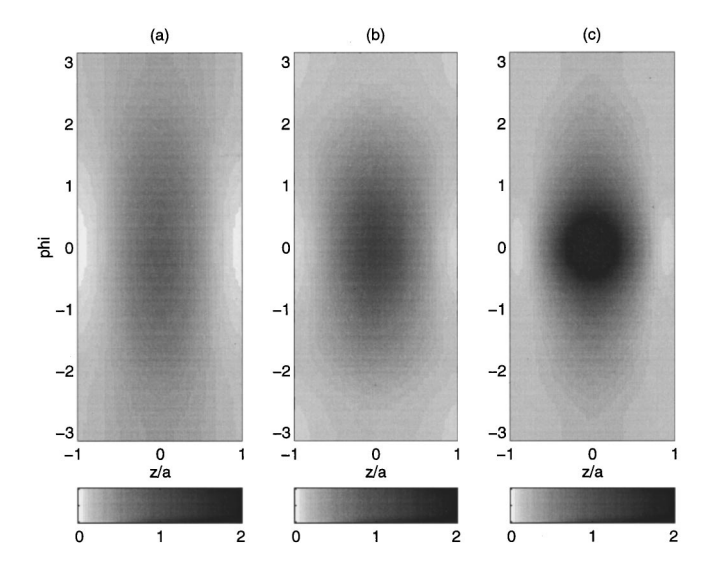


FIG. 3. The same data as shown in Fig. 2, i.e., $\rho' = 0.5a$ and ka = 3. (a)–(c) correspond to the same items in Fig. 2.

Before presenting the bad news regarding the "improved" imaging formulas, (34) and (35), we note that the low values of the maximum amplitude of the imaged intensity can be expected from the simple nature of the algorithm. Thus as the monopole source approaches the surface $(\rho' \rightarrow a)$ both the pressure and the velocity on the surface become singular, but the simple imaging relation predicts finite values. In fact, using Eqs. (3), (5), and (36) with $\rho' = a$, it gives

$$\hat{I}^{(s)}(0,0) = \frac{k}{4\pi a \rho_f c} \int_0^{\pi} d\theta (\sin \theta)^{1/2} \int_0^{\pi} d\theta' (\sin \theta')^{3/2}$$

$$= \frac{k}{3a\rho_f c} \quad \text{for } \rho' = a. \tag{37}$$

Hence the ratio of the imaged to the true intensity is

$$\frac{\hat{I}^{(s)}(0,0)}{I^{(s)}(0,0)} = \frac{2k}{3a}(a - \rho')^2 \quad \text{as } \rho' \to a.$$
 (38)

This is consistent with numerical simulations by Williams⁶ who found that the imaged intensity is generally well below the actual supersonic acoustic intensity in magnitude, although it gives the correct overall pattern or image. The result (38), combined with the conservation of energy for the simple imaging algorithm implies that the energy not imaged at the "hot spot" must be redistributed elsewhere on the surface. It is clear from the numerical examples, such as Fig. 2, that the energy redistribution does not occur within a distance of one acoustic wavelength. We can only infer that the approximate formula leads to an enhanced "background" imaged intensity.

Figures 4 and 5 show the comparison of the imaging formulas at higher frequencies using gray scale mosaics similar to Fig. 3. These figures illustrate a serious problem with the "improved" approximation of Eqs. (34) and (35): The second derivatives of F with respect to ϕ tend to dominate and make the correction far larger than the leading-order approximation. This results in the dumbbell appearance of

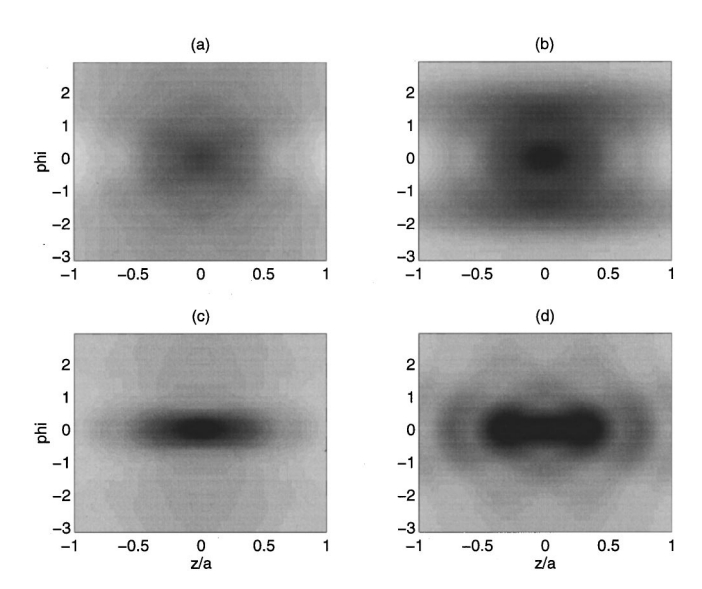


FIG. 4. The approximate, "improved approximate," and exact supersonic acoustic intensity, (a), (b), and (d), respectively, for $\rho' = 0.5a$ and ka = 9. The data in (c) were obtained by solving Eq. (39) by finite differences.

Fig. 5(b), for instance, which is clearly unrepresentative of the actual intensity. The problem with the derivatives of F can be avoided as follows. Ignoring the smaller-order terms, (32) can be written as

$$\hat{P} - \mu^{-2} \hat{P}_{\phi \phi} = \hat{P}^{(0)}(k \cos \theta, \phi), \tag{39}$$

where

$$\hat{P}^{(0)}(k \cos \theta, \phi) = e^{i(ka \sin \theta + \pi/4)} \sqrt{\frac{2\pi}{ka \sin \theta}}$$

$$\times \left(1 - \frac{1}{8ika \sin \theta}\right)^{-1} F(\theta, \phi) \quad (40)$$

and

$$\mu^2 = -\frac{1}{4} + 2ika \sin \theta. \tag{41}$$

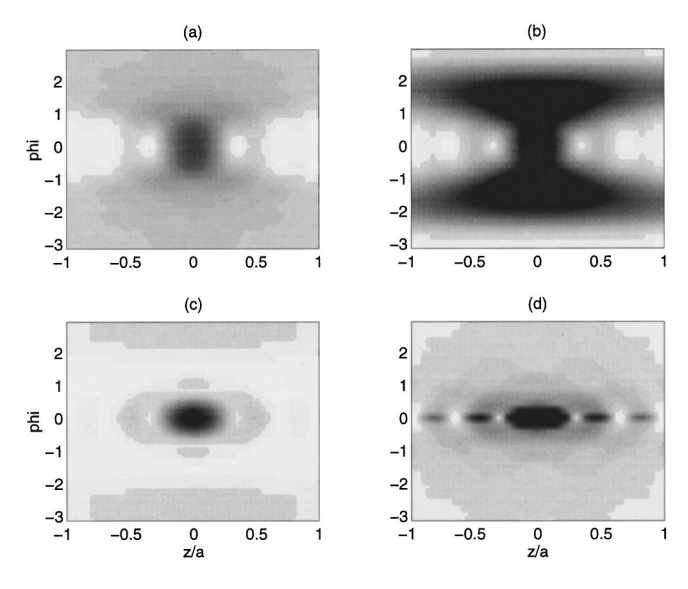


FIG. 5. The same as in Fig. 4 but for $\rho' = 0.9a$ and ka = 9.

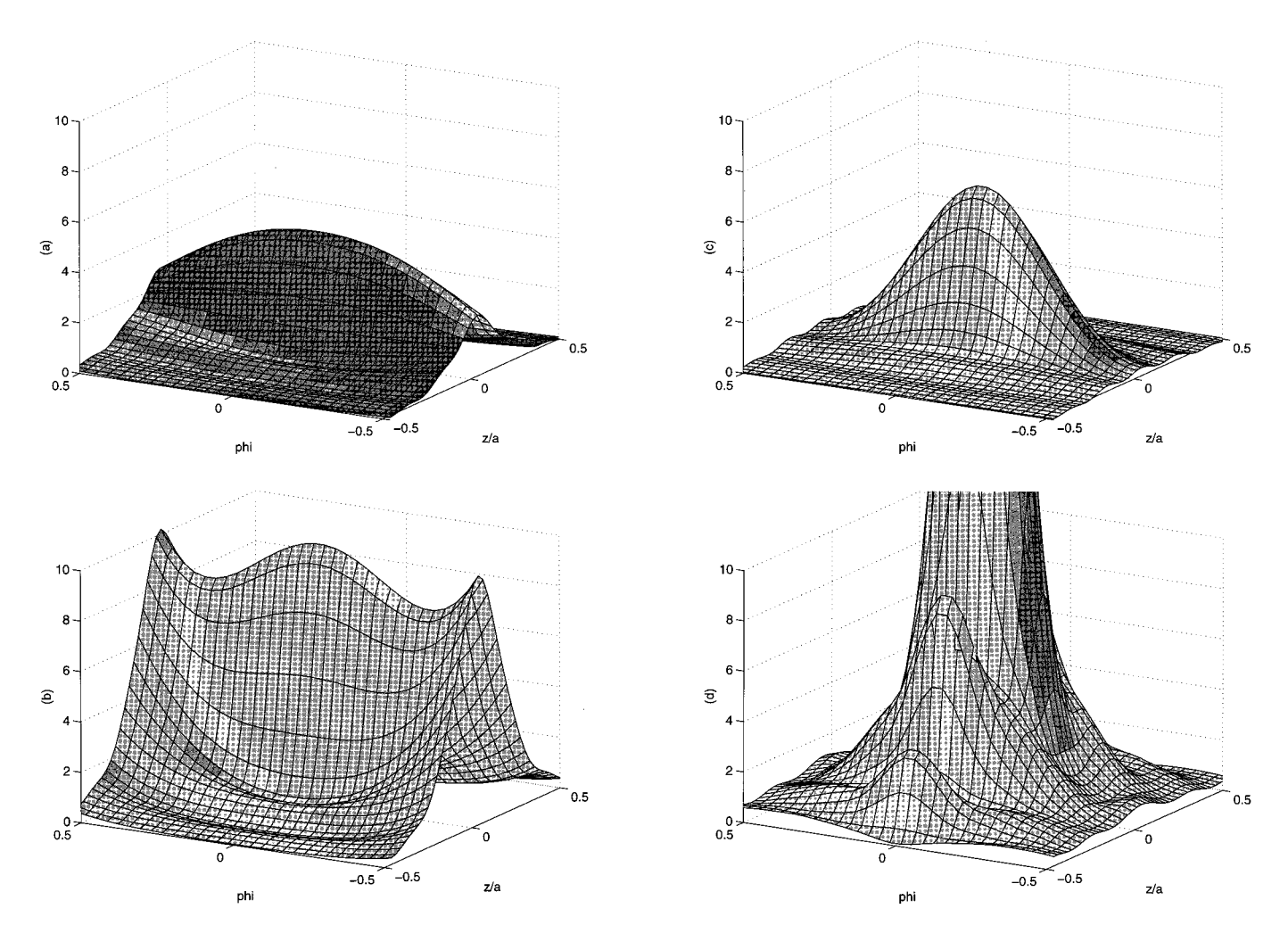


FIG. 6. The approximate, "improved approximate," finite difference solution, and the exact supersonic acoustic intensity, (a), (b), (c), and (d), respectively, for $\rho' = 0.9a$ and ka = 18. The difference scheme uses 30 equally spaced points on $-\pi/6 \le \phi \le \pi/6$.

Apart from the factor $[1-1/(8ika \sin \theta)]^{-1}$, which is close to unity in general, the function $\hat{P}^{(0)}(k \cos \theta, \phi)$ is exactly the leading-order approximation of Eq. (15), or Williams' formula. The images in Figs. 4(c) and 5(c) were obtained by solving Eq. (39) on a grid of 30 equally spaced ϕ points using finite differences as described below. The improved resolution illustrates that the second derivatives of F mentioned previously are indeed the culprit for the poor images in Figs. 4(b) and 5(b), and that a naive inversion of the basic formula (32) can lead to significant error.

The price paid by solving Eq. (39) is that the imaging formula is no longer strictly local. One can argue that if we are using all the data for $-\pi \le \phi \le \pi$ then we may as well use the exact modal algorithm (see the Appendix). However, the second-order equation (39) can be solved, in principle, on any interval by several methods: Green's functions, finite differences, etc. We will assume for simplicity that the farfield data is obtained on a set of semicircles evenly spaced in ϕ , say $\phi_j = \phi_1 + (j-1)\Delta\phi$, j=1,2,...,M, where $\Delta\phi$ is the azimuthal spacing. Let $\hat{P}_j = \hat{P}(k\cos\theta,\phi_j)$ and $\hat{P}_j^{(0)} = \hat{P}^{(0)} \times (k\cos\theta,\phi_j)$, then Eq. (39) is approximated by the central difference scheme

$$\hat{P}_{j} - \frac{1}{\mu^{2} (\Delta \phi)^{2}} [\hat{P}_{j+1} - 2\hat{P}_{j} + \hat{P}_{j-1}] = \hat{P}_{j}^{(0)},$$

$$j = 1, 2, ..., M.$$
(42)

The results shown in Figs. 4(c) and 5(c) for $-\pi \le \phi \le \pi$ were obtained using this scheme combined with periodic end conditions, which imply $\phi_0 = \phi_M$ and $\phi_{M+1} = \phi_1$. The results in Figs. 6(c), 7(c), and 8(b) were computed for the sector $-\pi/6 \le \phi \le \pi/6$ using similar periodicity conditions to evaluate the scheme at the end points. Other end conditions were tested and it was found that the numerical solutions were not sensitive to the precise form of the conditions used.

The results of Figs. 6(c), 7(c), and 8(b) indicate that better circumferential resolution can be expected if the simple differencing algorithm is adopted. The improvement in the resolution is quite remarkable even with very few semicircles of data, only seven in Fig. 8(b). Some understanding of the effect of using Eq. (39) can be obtained by noting that at high frequencies the real part of μ is large and positive, implying that the second derivative term in (39) acts as a singular perturbation, analogous to a boundary layer

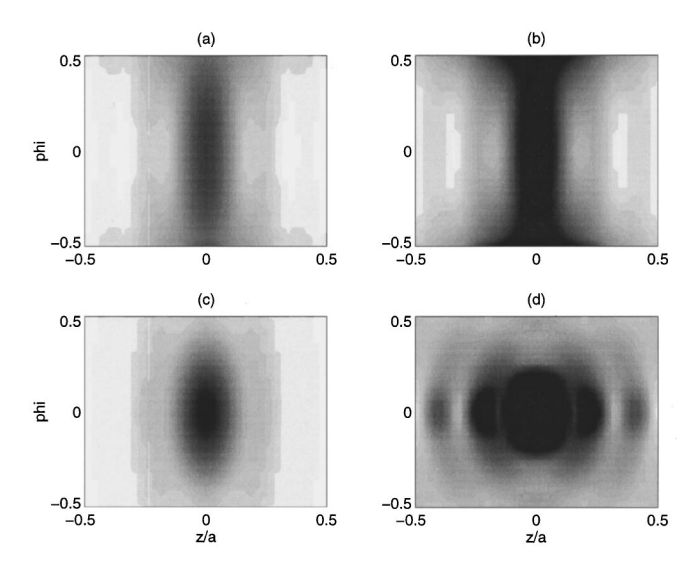


FIG. 7. The results of Fig. 6 depicted by gray scale mosaic.

effect. By ignoring the fact that the range of ϕ is finite, and replacing the domain by the full line, with zero boundary conditions at $\pm \infty$, we may write the solution to (39) as

$$\hat{P}(k \cos \theta, \phi) = \frac{\mu}{2} \int_{-\infty}^{\infty} d\phi' e^{-\mu|\phi - \phi'|} \hat{P}^{(0)}(k \cos \theta, \phi').$$
(43)

Integrating by parts yields

$$\hat{P}(k \cos \theta, \phi) = \hat{P}^{(0)}(k \cos \theta, \phi) + \frac{1}{2} \int_{0}^{\infty} d\phi' e^{-\mu\phi'} [\hat{P}^{(0)}_{,\phi}(k \cos \theta, \phi + \phi') - \hat{P}^{(0)}_{,\phi}(k \cos \theta, \phi - \phi')].$$
(44)

This form clearly shows the leading-order term $\hat{P}^{(0)}$, and the boundary layer correction, within a region of azimuthal thickness $1/\text{Re}\mu = O(1/\sqrt{ka \sin \theta})$.

III. CONCLUSION

The imaging formula of Williams is practical and very useful because it provides a simple means to map the far-field pressure back to a cylindrical surface. The power of the method is that it is local, and does not require full circumferential coverage. Data from each semi-circular scan is back projected independently. In this paper we have seen that the same formula can be generalized to cylinders of arbitrary cross section, with the main results being Eqs. (3) and (5). The cross section need not be a separable surface. In fact, the derivation relies upon a local, high-frequency approximation which illustrates that the formula is really the leading order of an asymptotic approximation. We also obtained the first two terms in the asymptotic series for the special case of a circular cylinder. One can, in principle, continue the asymptotic series for arbitrary cross section.

The two-term approximation can be interpreted in two ways. By the nature of its derivation it gives the surface pressure transform P as the solution of a differential equation, Eq. (32). This can be formally solved, in the spirit of

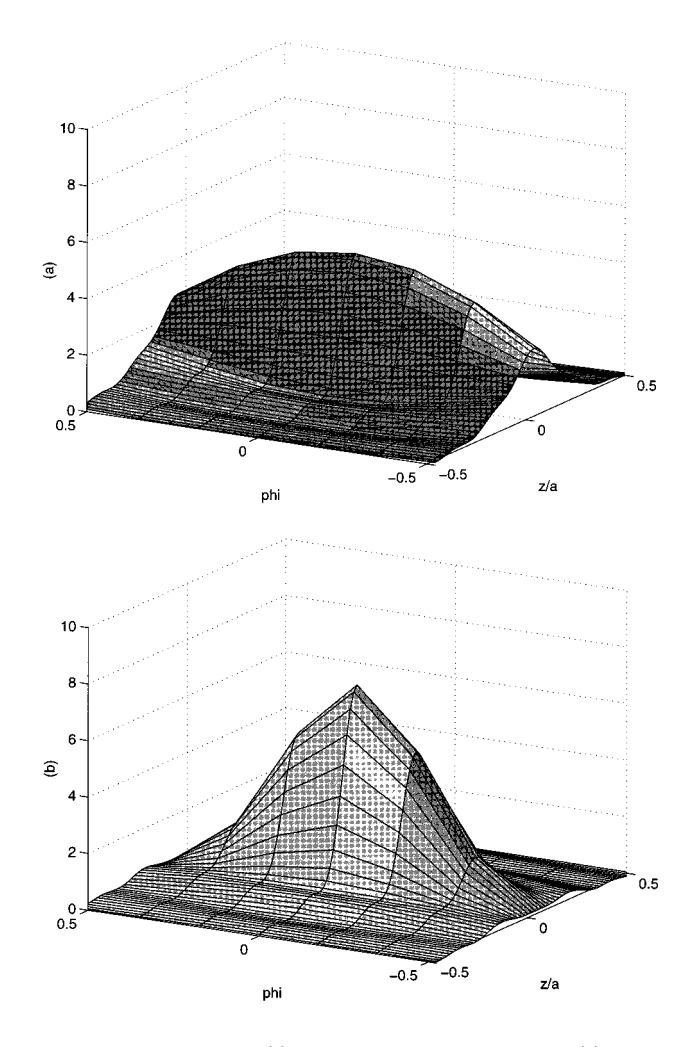


FIG. 8. The approximate, (a), and finite difference solution, (b), for the same parameters as Fig. 6, except that only seven equally spaced ϕ points are used.

the asymptotic approximation, yielding a direct and local imaging formula, Eq. (33), which introduces a correction to Williams' formula. However, as the numerical examples illustrate, this "improved" scheme is actually worse than the original, and the cause of the problem lies with the second-order derivatives with respect to ϕ , which is also related with the ill-posed nature of the inverse problem (see the Appendix). The proper interpretation of the asymptotic correction is as a nonlocal effect, which must be solved as such. One approach is to use finite differences for sets of several neighboring semicircles. The numerical examples for a monopole near the surface indicate that even with very few semicircles one can gain significant resolution in the circumferential direction, as compared with the simple local imaging formula.

ACKNOWLEDGMENTS

My thanks to Earl Williams for comments. This work was supported by the Office of Naval Research.

APPENDIX: THE CIRCULAR CYLINDER

The special case of constant $b(\phi) = a$ is considered here. It may be easily shown, using modal expansions for instance, that the z-transformed surface velocity can be expressed in terms of the surface pressure as

$$V(k \cos \theta, \phi) = \frac{\sin \theta}{\rho_f c} \int_0^{2\pi} d\phi' G(\theta, \phi - \phi') P(k \cos \theta, \phi'),$$
(A1)

where

$$G(\theta, \phi - \phi') = \sum_{n = -\infty}^{\infty} -i \frac{H_n^{(1)'}(ka \sin \theta)}{H_n^{(1)}(ka \sin \theta)} e^{in(\phi - \phi')}.$$
(A2)

Assuming that $ka \sin \theta \gg 1$ we can use the following asymptotic approximation for the Hankel functions,

$$H_n^{(1)}(x) = (-i)^{n+1} e^{i(x+\pi/4)} \sqrt{\frac{2}{\pi x}} \left[1 + i \frac{(4n^2 - 1)}{8x} + \cdots \right].$$
(A3)

By retaining the first two terms in the expansion of $-iH_n^{(1)}(y)/H_n^{(1)}(y)$ for $y \ge |n|$, we obtain

$$\hat{G}(\theta, \phi - \phi') = \delta(\phi - \phi') \left(1 - \frac{1}{8ika \sin \theta} \right) + \cdots$$
 (A4)

Equations (A1) and (A4) together imply Eq. (11) for the special case of the circular cylinder.

Substituting from (A1) into the Helmholtz integral (8) and using standard identities for Bessel and Hankel functions, we obtain the exact relationship between the far-field form function and the surface pressure transform,

$$F(\theta,\phi) = \frac{1}{2\pi} \int_0^{2\pi} d\phi' P(k \cos \theta, \phi')$$

$$\times \sum_{n=-\infty}^{\infty} \frac{e^{in(\phi-\phi')}}{\pi(i)^{n+1} H_n^{(1)}(ka \sin \theta)}.$$
(A5)

This derivation is related to, and motivated by, that of Williams. The distinction is that Williams essentially obtained $P(k\cos\theta,\phi)$ directly. There is a slight complication with his approach, which is based upon the fact that the near-to-far-field radiation operator is compact. In order to appreciate this difficulty, define the functions $L_N^{(\pm 1)}(\phi-\phi',\theta)$ as

$$L_N^{(\pm 1)}(\phi - \phi', \theta) = \sum_{n=-N}^{N} \left[\pi(i)^{n+1} H_n^{(1)} \right] \times (ka \sin \theta)^{-1} e^{in(\phi - \phi')}, \tag{A6}$$

then Eq. (A5) is equivalent to

$$F(\theta, \phi) = \frac{1}{2\pi} \int_0^{2\pi} d\phi' \ P(k \cos \theta, \phi') L^{(1)}(\phi - \phi', \theta),$$
(A7)

where $L^{(1)} = \lim_{N \to \infty} L_N^{(1)}$. It follows from the small argument or large order form of the Hankel functions, $H_n^{(1)}(x) = (-1/\pi)(2/x)^n(n-1)! + \cdots$, that the function $L^{(1)}(\phi - \phi', \theta)$ is convergent and well defined. We note in passing that the precise form function requires the infinite sum, in general, and is not defined by the integral using the truncated version $L_N^{(1)}$, where N is approximately $ka \sin \theta$. As a counter example, consider a set of m monopoles, equally spaced azimuthally at $\phi_i = 2\pi j/m$ with amplitudes $e^{im\phi_j}$, i

=1,2,...,m. For large m the dominant contribution to $F(\theta,\phi)$ comes from n=m, which would not be picked up if we used the truncated form of $L^{(1)}$.

Let $F_N(\theta, \phi)$ be the function obtained using the truncated function $L_N^{(1)}$ in the integral in Eq. (A7) instead of $L^{(1)}$. The same function is obtained by using the 2N+1 modal expansion of $P(k \cos \theta, \phi')$, say $P_N(k \cos \theta, \phi')$, as the integrand in Eq. (A7), i.e.,

$$\begin{split} F_{N}(\theta,\phi) &= \frac{1}{2\pi} \int_{0}^{2\pi} d\phi' \ P(k \cos \theta,\phi') L_{N}^{(1)}(\phi - \phi',\theta) \\ &= \frac{1}{2\pi} \int_{0}^{2\pi} d\phi' \ P_{N}(k \cos \theta,\phi') L_{N}^{(1)}(\phi - \phi',\theta) \\ &= \frac{1}{2\pi} \int_{0}^{2\pi} d\phi' \ P_{N}(k \cos \theta,\phi') L^{(1)}(\phi - \phi',\theta), \end{split} \tag{A8}$$

and conversely,

$$P_{N}(k \cos \theta, \phi) = \frac{1}{2\pi} \int_{0}^{2\pi} d\phi' \ F_{N}(\theta, \phi') L_{N}^{(-1)}(\phi - \phi', \theta). \tag{A9}$$

However, we cannot take the limit of $N \to \infty$ in this equation, because, although $P_N \to P$ and $F_N \to F$, the limit of $L_N^{(-1)}$ as $N \to \infty$ does not converge at any point, and hence it is not a well-defined function. In summary, any m-mode limited form of $F(\theta, \phi)$ can be inverted to give the corresponding m-mode form of $P(k \cos \theta, \phi)$. The inversion process is stable for $m \le N$, where $N \approx ka \sin \theta$, and is unstable for larger m, even though the dominant contribution to F could be from modes with m > N. The lack of an explicit integral formula for $P(k \cos \theta, \phi)$ is a consequence of the fact that the integral operator in Eq. (A7) is compact, and as such, has no inverse. The ill-posedness of this type of inverse problem is common, and methods exist to regularize the problem.

If $ka \sin \theta \gg N \gg 1$, then the following approximations can be obtained from (A3),

$$L_N^{(\pm 1)}(\phi - \phi', \theta) = 2\pi e^{\pm i(ka\sin\theta + \pi/4)}$$

$$\times \left[\frac{2\pi}{ka\sin\theta}\right]^{\pm 1/2} \left[\delta(\phi - \phi')\right] 1$$

$$\pm \frac{1}{8ika\sin\theta} \pm \frac{\delta''(\phi - \phi')}{2ika\sin\theta} + \cdots \right].$$
(A10)

We have also used the approximation $\sin(\lambda x)/(\pi x) \approx \delta(x)$ for sufficiently large λ . The approximations of Eq. (32) for F in terms of P follows from Eq. (A7) combined with Eq. (A10) for $L_N^{(1)}$ in the limit $N \rightarrow \infty$. However, as remarked above, we cannot take the same limit for $L_N^{(-1)}$, although formally doing so yields Eq. (33) from Eqs. (A10) and (A9).

Finally, we note that the numerical examples use the following representation for a monopole located at (ρ, z, ϕ) = $(\rho', 0, 0)$, $\rho' \le a$,

$$p^{(s)}(z,\phi) = \frac{ik}{2} \int_0^{\pi} d\theta \sin \theta e^{ikz \cos \theta} \sum_{n=-\infty}^{\infty} e^{in\phi} H_n^{(1)}$$
$$\times (ka \sin \theta) J_n(k\rho' \sin \theta). \tag{A11}$$

- ³G. Borgiotti, A. Sarkissian, E. G. Williams, and L. Schuetz, "Conformal generalized near-field acoustic holography for axisymmetric geometries," J. Acoust. Soc. Am. 88, 199–209 (1990).
- ⁴ A. Sarkissian, "Reconstruction of the surface acoustic field on radiating structures," J. Acoust. Soc. Am. **92**, 825–830 (1992).
- ⁵D. M. Photiadis, "The relationship of singular value decomposition to wave-vector filtering in sound radiation problems," J. Acoust. Soc. Am. **88**, 1152–1159 (1990).
- ⁶E. G. Williams, "Imaging the sources on a cylindrical shell from far-field pressure measured on a semicircle," J. Acoust. Soc. Am. 99, 2022–2032 (1996).
- ⁷E. G. Williams, "Supersonic acoustic intensity," J. Acoust. Soc. Am. **97**, 121–127 (1995).
- ⁸ A. Sarkissian, "Acoustic radiation from finite structures," J. Acoust. Soc. Am. 90, 574–578 (1991).
- ⁹D. L. Colton and R. Kress, *Integral Equation Methods in Scattering Theory* (Wiley, New York, 1993).

¹E. G. Williams, H. D. Dardy, and K. B. Washburn, "Generalized nearfield acoustic holography for cylindrical geometry: Theory and experiment," J. Acoust. Soc. Am. **81**, 389–504 (1987).

²W. A. Veronesi and J. D. Maynard, "Digital holographic reconstruction of sources with arbitrarily shaped surfaces," J. Acoust. Soc. Am. 85, 588–598 (1988).